Time-Resolved Pump–Probe Imaging of Ablation Phenomena in Silica Glass Using Visible Femtosecond Laser

E. Terasawa[*1,2], D. Satoh[2,3], T. Shibuya[3], Y. Moriai[2], H. Ogawa[2,3], M. Tanaka[2,3], K. Sakaue[1,4], M. Washio[1], Y. Kobayashi[2,5], and R. Kuroda[2,3]

[1]*Waseda Research Institute for Science and Engineering, Waseda University, Japan*
[2]*AIST-UTokyo Advanced Operando-Measurement Technology Open Innovation Laboratory (OPERANDO-OIL), National Institute of Advanced Industrial Science and Technology (AIST), Japan*
[3]*Research Institute for Measurement and Analytical Instrumentation (RIMA), National Metrology Institute of Japan (NMIJ), National Institute of Advanced Industrial Science and Technology (AIST), Japan*
[4]*Photon Science Center, Graduate School of Engineering, The University of Tokyo, Japan*
[5]*The Institute for Solid State Physics, The University of Tokyo, Japan*
[*]*Corresponding author's e-mail: wisdom_terasawa@akane.waseda.jp*

The ablation phenomena in silica glass were investigated using a visible femtosecond laser and time-resolved pump–probe imaging. A pump pulse with a wavelength of 400 nm was employed. Only gentle ablation occurred at a peak fluence of 6.88 J/cm^2, and gentle ablation and strong ablation occurred at a peak fluence of 8.23 J/cm^2. At both peak fluences, reflectivity increased owing to excitation at a delay time of ~1 ps. At a delay time of ~30 ps, a decrease in reflectivity due to melting was observed only at the local fluence that generated strong ablation. The ablation that occurred after melting was considered to correspond to strong ablation. Similar changes in reflectivity were observed for two values of the local fluence that corresponded to gentle ablation.

DOI: 10.2961/jlmn.2021.03.2008
Keywords: pump–probe imaging, femtosecond laser ablation, silica glass, visible wavelength, laser processing

1. Introduction

The laser ablation phenomenon induced by a femtosecond laser should allow for the high-precision processing of any material with an extremely reduced heat effect [1]. Silica glass has excellent properties such as high purity, transparency, and chemical resistance. Femtosecond laser processing has the potential to solve a problem that it is difficult to achieve the high-precision processing of silica glass with mechanical machining or conventional laser processing (continuous wave lasers and pulsed lasers with pulse durations of a few nanoseconds or more). To achieve the high-precision processing with femtosecond lasers, it is necessary to optimize laser processing parameters (wavelength, pulse duration, pulse energy, repetition rate, spot size, number of shots, polarization, etc.) according to the type and shape of a material. Nevertheless, several studies on the femtosecond laser processing of silica glass have usually employed wavelengths in the near-infrared regime (for example, 800 nm and 1030 nm). Thus, it is important to evaluate the processing characteristics at other wavelengths and elucidate the mechanism to predict processing phenomena.

In a previous study, we have investigated the ablation threshold of silica glass in the visible femtosecond regime to achieve high-quality and efficient processing using a wavelength of 400 nm [2]. Two affected regimes has been confirmed in an ablated crater, i.e., "gentle ablation'' and "strong ablation,'' which have been explained using Coulomb explosion [3,4] and phase explosion [5], respectively. In the craters that are formed by these phenomena, the rim of one of the melting traces created by strong ablation [6] is covered by a shallow crater created by gentle ablation. The formation of the rim on the shallow crater suggests that the shallow crater and rim are formed at different times. This implies that the two ablations resulting from this crater shape occur in different time regimes.

Pump–probe imaging has been used to measure laser-induced ablation phenomena, including excitation, melting, and surface deformation in metals [7–9], semiconductors [7,8,10], dielectric materials [7,11–16], and polymers [8]. This method has revealed that excitation occurs first, and it increases reflectivity based on the Drude model [10,11,15,17]. Then, as excited electrons are trapped as exciton or, energy is transferred to a lattice system and melting begins. The reflectance of this molten state is lower than that of the sample surface [8,9]. Subsequently, the material expands. At this time, signs of Newton's rings and a rarefaction wave are confirmed [10,14,15]. These measurement results vary depending on the material and laser parameters [9,17]. However, it is still unknown about dynamics of gentle ablation phenomena. In this study, we investigated the dynamics of the femtosecond laser ablation phenomena, i.e., gentle ablation and strong ablation, in silica glass using pump–probe imaging equipment with a femtosecond laser that used a wavelength of 400 nm for the pump pulse.

2. Experimental methods

2.1 Pump–probe imaging system

We conducted time-resolved reflective imaging using pump–probe microscopy. Fig. 1 shows the schematic of the experimental setup. The femtosecond laser source was a Ti:sapphire regenerative amplifier based on chirped pulse amplification. This source delivered femtosecond laser pulses at a center wavelength of 800 nm with a Gaussian beam. The pulse duration was set as 400 fs by varying the diffraction grating distance to generate two affected regimes, i.e., gentle ablation and strong ablation (the details of the laser parameters are provided in Section 4.2). The femtosecond laser pulse was divided into pump and probe pulses by utilizing the combination of a half-wave plate (HWP1) and a thin-film polarizer (TFP1). The wavelength of the pump pulse was converted to 400 nm using a barium borate (BBO) crystal, and its energy was adjusted using a combination of a half-wave plate (HWP2) and a thin-film polarizer (TFP2) before the BBO crystal. The pump pulse was focused by a plano-convex lens (CL1) with a focal length of 75 mm and irradiated on the sample surface of silica glass at an incident angle of 55° with s-polarization. The beam shape and ablation crater became elliptical because of the oblique irradiation. The beam waist radii ($1/e^2$) were obtained as ω_x = 11 μm and ω_y = 4.6 μm using the Liu plot [18], and the ellipticity was 0.42.

The probe pulse divided by TFP1 was used for the microscopic observation of the ablation dynamics generated by the pump pulse with a wavelength of 400 nm. The probe beam profile was converted to the Gaussian profile by eliminating the high-order mode using a spatial filter consisting of a tungsten pinhole (50 μm diameter) and two convex lenses. The time delay between the pump and probe pulses could be adjusted up to 1.2 ns by an optical delay line between 200 mm with a minimum step size of 2 μm. The microscopic observation was performed using a microscope objective lens (50×, N.A. = 0.42, W.D. = 17.0 mm). A plano-convex lens (CL2) placed behind the microscope objective lens focused the probe beam to provide collimated illumination on the sample surface. The reflected light from the sample passed through the objective lens again and was guided to the imaging system by a thin-film polarizer (TFP3) and quarter-wave plate (QWP1). In the imaging system, a band-pass filter (center wavelength of 800 nm) eliminated the pump light with a wavelength of 400 nm and the plasma emission generated during the ablation. The image was focused using a tube lens (TL, f = 200 mm) and captured by a 12-bit complementary metal–oxide–semiconductor camera.

The time zero between the pump and probe at the delay time was determined using the optical Kerr effect. This method has been generally used in pump–probe experiments on transparent dielectric materials such as silica glass and sapphire [17]. Fig.2 depicts the system used for measuring the optical Kerr effect signal. The probe pulse transmitted from the sample was measured using a photodetector (PD) placed after the polarizer of a Glan laser prism (GLP). The probe light was linearly polarized by a quarter-wave plate (QWP2), and the polarizer was arranged in a crossed-Nicol state. The angle of polarization between the pump and probe light was ±45°. A quarter-wave plate (QWP3) was placed before the barium borate (BBO) crystal to compensate for the delay caused by QWP2. When the delay time was varied, the peak light intensity detected by the photodetector was defined as the time zero. This time zero represented the time at which the peaks of the pump pulse and probe pulse overlapped.

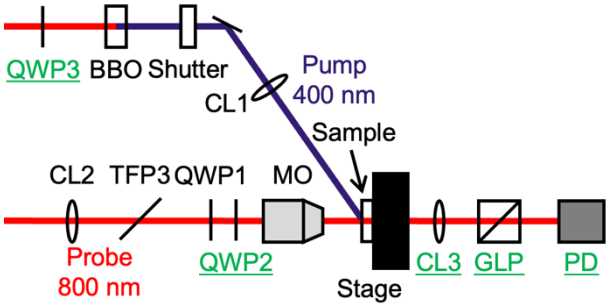

Fig. 2 System used for measuring the optical Kerr effect signal. Abbreviations: GLP—Gran laser prism, PD—photo detector.

2.2 Sample and laser processing parameters

The sample was used to silica glass (23 mm × 23 mm × 1 mm, double-sided mirror surface, AGC: Synthetic Fused Silica Glass AQ) and placed on a 3-axis stage. Single-shot pump pulse irradiation was used to eliminate the influence of the incubation effect.

The pulse duration of the pump pulse was set as 400 fs. Additionally, the peak fluence was set as 6.88 J/cm^2 and 8.23 J/cm^2 to measure gentle ablation and strong ablation,

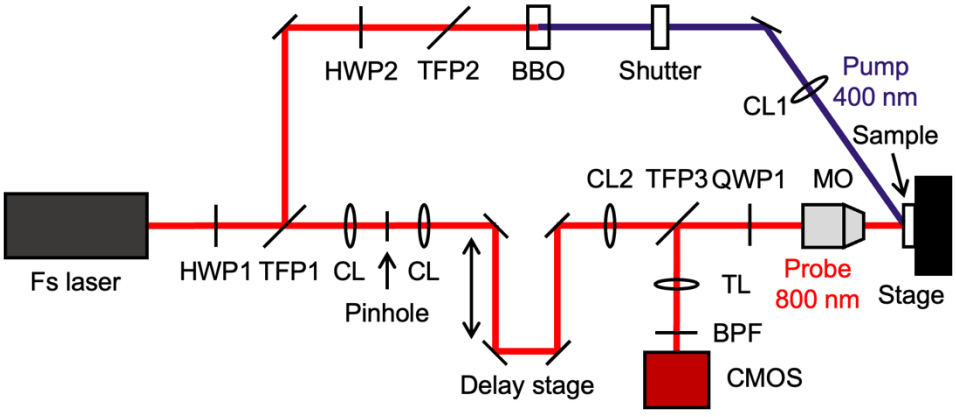

Fig. 1 Experimental setup of pump–probe imaging. Abbreviations: HWP—half-wave plate, TFP—thin-film polarizer, CL—convex lens, QWP—quarter-wave plate, TL—tube lens, MO—microscope objective, BPF—band-pass filter.

respectively. Here, peak fluence represents the pump pulse focused just before the surface of the silica glass sample. Fig. 3 (a, c) shows the crater irradiated by a 400-fs pulse with a peak fluence of 6.88 J/cm^2; the crater is approximately 3.4 μm wide and 50 nm deep. This corresponds to only gentle ablation [2]. Fig. 3 (b, d) shows the crater irradiated with a peak fluence of 8.23 J/cm^2. This crater shows two affected regimes: a regime that is approximately 3.8 μm wide and 130 nm deep on the inside and a shallow regime that is approximately 4.9 μm wide and 30 nm deep on the outside. These correspond to strong ablation and gentle ablation [2]. Under the conditions of these pump pulses, time-resolved measurements were conducted using the pump–probe imaging system shown in Fig. 1.

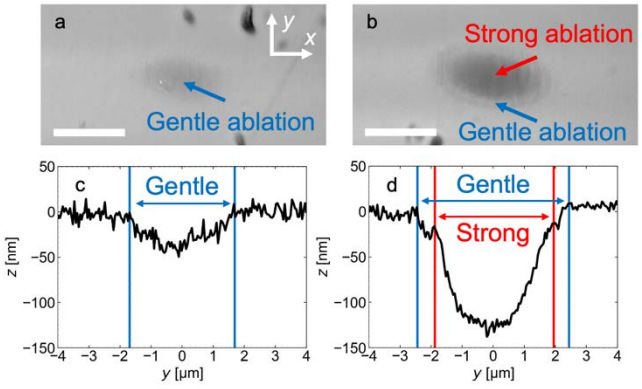

Fig. 3 Craters irradiated by a 400-fs pulse with peak fluence of (a, c) 6.88 J/cm^2 and (b, d) 8.23 J/cm^2 measured using a laser confocal microscope. Cross sections of these craters along y-axis at x = 0. The white bar represents 5 μm.

3. Results and discussion

Fig. 4 shows the time-resolved reflection images on silica glass for various delay times. The peak fluence for the images in the top and bottom rows is 6.88 J/cm^2 and 8.23 J/cm^2, respectively. The reflectivity increases at ~1 ps, which indicates free electron generation by excitation [17]. Then, the reflectivity decreases after ~ 1ps. However, it is not less than the reflectivity of the nonirradiated surface of the sample for a peak fluence of 6.88 J/cm^2. In contrast, it is less than the reflectivity of the nonirradiated surface of the sample for a peak fluence of 8.23 J/cm^2. This has been reported to be an indication of melting [8,9].

Fig. 5 shows a plot of the reflectivity vs. the delay time at three positions in the time-resolved reflection images shown in Fig. 4. The first position, (A), is the center of the image at a peak fluence 6.88 J/cm^2. The second position, (B), is the center of the image at a peak fluence of 8.23 J/cm^2. The third position, (C), is located at a distance of y = -2.0 μm from the center at a peak fluence 8.23 J/cm^2. The change in reflectivity is defined as

$$\frac{\Delta R}{R_0} = \frac{R(t)-R_0}{R_0} \quad (1)$$

where R_0 and $R(t)$ are the reflectivities of the nonirradiated and irradiated surfaces, respectively. (C) corresponds to the location of gentle ablation in Fig. 3 (b, d). The local fluence at this position is 5.64 J/cm^2, which is lower than the strong ablation threshold (F_{th} = 7.80 J/cm^2) obtained using the Liu plot. The reflectivity increases at a delay time of ~1.5 ps, which indicates the generation of free electrons by laser-induced excitation: $\Delta R/R_0$ = 5.92, 7.77, and 4.69 at (A), (B), and (C), respectively. The decrease in reflectivity to less than that of the nonirradiated surface at approximately 30 ps is an indication of melting. This decrease is only confirmed in the region where strong ablation occurs at (B), with $\Delta R/R_0$ ~ -0.5. Therefore, the ablation that occurs after melting is

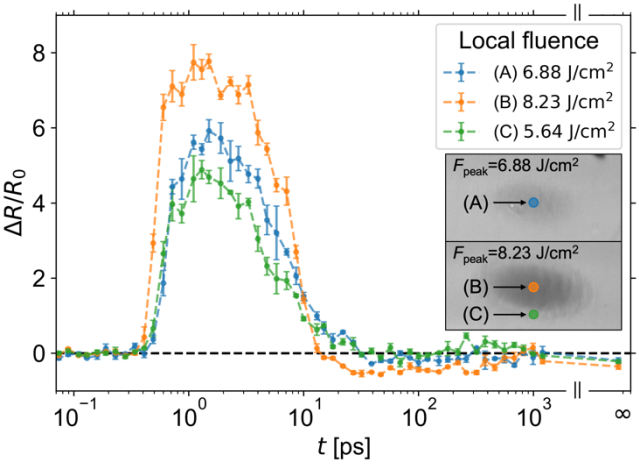

Fig. 5 Changes in reflectivity ($\Delta R/R_0$) with delay time at three positions on time-resolved reflection images. (A) is on the crater generated by pulse with peak fluence of 6.88 J/cm^2. Local fluence at (A) is 6.88 J/cm^2. (B) and (C) are on the crater generated by pulse with peak fluence of 8.23 J/cm^2. Local fluence at (B) and (C) is 8.23 J/cm^2 and 5.64 J/cm^2, respectively. The error bars represent the corrected standard deviations calculated from three reflection images under the same experimental conditions.

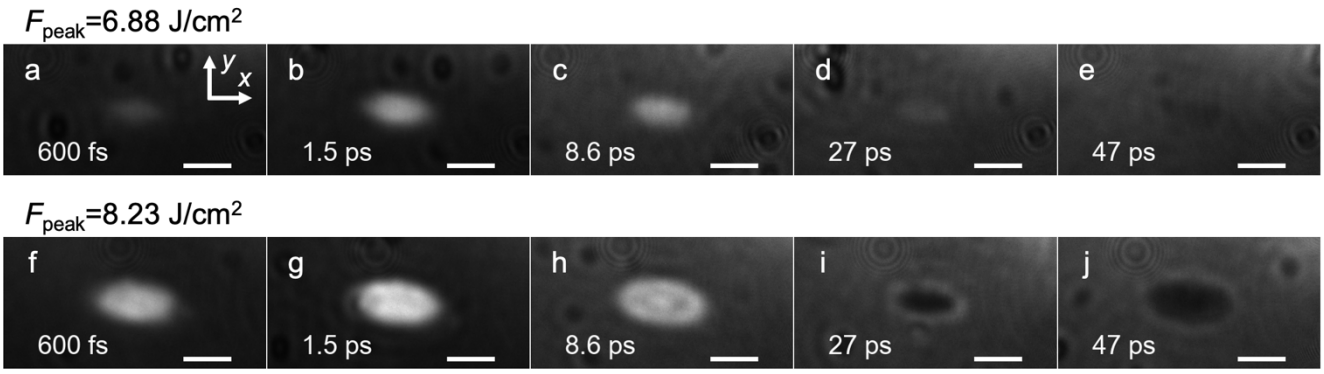

Fig. 4 Time-resolved reflection images of silica glass after the pump-pulse irradiation at various delay times. (a–e) Top and (f–j) bottom rows are for a peak fluence of 6.88 J/cm^2 and 8.23 J/cm^2, respectively. The white bar represents 5 μm.

considered as strong ablation. The reflectivities, $\Delta R/R_0$, of the final state, which was obtained at a delay time of ∞, was -0.196, -0.354, and -0.216 at (A), (B), and (C), respectively.

The positions (A) and (C) correspond to the affected areas where only gentle ablation occurred. The changes in the reflectivities at these positions were similar. The reflectivity increased at ~1.5 ps and then decreased. However, this decrease in the reflectivity was not less than that of the nonirradiated surface, at approximately 30 ps. Thus, the changes in reflectivity corresponding to the gentle and strong ablations were different. Fig. 6 shows the normalized reflectivities—$(R\text{-}R_{min})/(R_{max}\text{-}R_{min})$ (i.e., normalized by the maximum and minimum intensities shown in Fig. 5). For a delay time of 10–40 ps, the trend in reflectivity reduction corresponding to gentle ablation ((A) and (C)) was different than that corresponding to the strong ablation ((B)). We can consider that the different reflectivity decay trends caused the irradiated sample to separate into two layers with different refractive indices. Based on this consideration, we can state that under gentle ablation, the sample surface separated into two layers—a high-reflection region, which resulted from excitation, and the unablated surface regions. Reflection was detected from both the layers (the inset of Fig. 6), indicating that the reflectivity decreased gradually. Bases on this analysis, the ring-shaped decrease in the reflectivity observed in Fig. 4 (h) can also be explained by the separation of the sample surface into two layers, viz. a high-reflection region induced by excitation and a low-reflection region generated by the melting [8,9].

As a transient change in reflectivity, it has been reported to change the material state by the rarefaction wave [10,14,15]. There is a difference between the change in reflectivity observed in this study and the changes in reflectivity as a result of the rarefaction wave. At a delay time of the rarefaction wave to reach the boundary between the ablation layer and the substrate, owing to the discontinuity between the rarefaction wave and the substrate, a temporary increase in reflectivity is observed [10]. In our experiments, this temporary increase in reflectivity was not observed. The reason why it was not observed is considered that the gentle ablation occurred without heating and melting and did not lead to the production of the rarefaction wave.

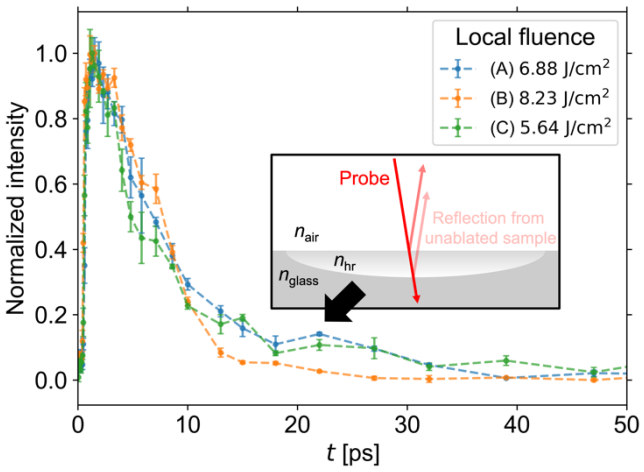

Fig. 6 Normalized reflectivity in Fig. 5. The inset shows the schematic of the irradiated sample separated into two layers with different refractive indices; n_{hr} is the high-reflection region created by excitation and n_{glass} is the unablated silica glass sample.

It has not been investigated these two ablations occurred at a wavelength of 400 nm also occur at other laser processing parameters (wavelength, spot size, etc.), and further investigation is still required to understand the dynamics of these ablation phenomena.

4. Conclusions

We investigated the temporal evolution of the laser-induced ablation phenomenon in silica glass using a femtosecond laser with a wavelength of 400 nm and time-resolved pump–probe imaging spectroscopy. Only gentle ablation occurred at a peak fluence of 6.88 J/cm^2. The change in reflectivity was evaluated at position (A) with a local fluence of 6.88 J/cm^2. Gentle and strong ablation occurred at a peak fluence of 8.23 J/cm^2. In this case, the change in reflectivity was evaluated at positions (B) and (C) with a local fluence of 8.23 J/cm^2 and 5.64 J/cm^2, respectively. The values of the local fluence corresponded to the affected regimes where gentle ablation and strong ablation occurred. At all three positions, reflectivity increased owing to free electron generation at delay time of ~1.5 ps: $\Delta R/R_0$ = 5.92, 7.77, and 4.69 at (A), (B), and (C), respectively. Then, at (B), reflectivity decreased to less than that of the nonirradiated surface ($\Delta R/R_0$ ~ -0.5) at a delay time of ~30 ps. It was considered that the ablation generated after melting corresponded to strong ablation. The changes in reflectivity were similar at (A) and (C), which corresponded to gentle ablation. The temporary decay trend changed around 20 ps at (A) and (C) because reflection was detected from the high-reflection region due to excitation and the unablated region of the sample.

Acknowledgments

This work is partly based on the results obtained from the New Energy and Industrial Technology Development Organization (NEDO) project “Development of advanced laser processing with intelligence based on high-brightness and high-efficiency laser technologies” (TACMI project).

References

[1] K.C. Phillips, H.H. Gandhi, E. Mazur, and S.K. Sundaram: Adv. Opt. Photonics., 7, (2015) 684.
[2] E. Terasawa, T. Shibuya, D. Satoh, Y. Moriai, H. Ogawa, M. Tanaka, R. Kuroda, Y. Kobayashi, K. Sakaue, and M. Washio: Appl. Phys. A., 126, (2020) 446.
[3] D. Ashkenasi, A. Rosenfeld, H. Varel, M. Wähmer, and E.E.B. Campbell: Appl. Surf. Sci., 120, (1997) 65.
[4] R. Stoian, A. Rosenfeld, D. Ashkenasi, I. V. Hertel, N.M. Bulgakova, and E.E. Campbell: Phys. Rev. Lett., 88, (2002) 097603.
[5] J. Perrière, C. Boulmer-Leborgne, R. Benzerga, and S. Tricot: J. Phys. D. Appl. Phys., 40, (2007) 7069.
[6] A. Ben-Yakar, A. Harkin, J. Ashmore, R.L. Byer, and H.A. Stone: J. Phys. D. Appl. Phys., 40, (2007) 1447.
[7] D. Von Der Linde, K. Sokolowski-Tinten, and J. Bialkowski: Appl. Surf. Sci., 109–110, (1997) 1.
[8] I. Carrasco-García, J.M. Vadillo, and J. Javier Laserna: Spectrochim. Acta - Part B At. Spectrosc., 113, (2015) 30.

[9] I.M. Carrasco-García, J.M. Vadillo, and J.J. Laserna: Spectrochim. Acta - Part B At. Spectrosc., 158, (2019) 105634.
[10] D. Satoh, T. Shibuya, E. Terasawa, Y. Moriai, H. Ogawa, M. Tanaka, Y. Kobayashi, and R. Kuroda: Appl. Phys. A., 126, (2020) 795.
[11] J. Siegel, D. Puerto, W. Gawelda, G. Bachelier, J. Solis, L. Ehrentraut, and J. Bonse: Appl. Phys. Lett., 91, (2007) 082902.
[12] J. Hernandez-Rueda, D. Puerto, J. Siegel, M. Galvan-Sosa, and J. Solis: Appl. Surf. Sci., 258, (2012) 9389.
[13] M. Garcia-Lechuga, J. Siegel, J. Hernandez-Rueda, and J. Solis: J. Appl. Phys., 116, (2014) 113502.
[14] M. Garcia-Lechuga, J. Siegel, J. Hernandez-Rueda, and J. Solis: Appl. Phys. Lett., 105, (2014) 112902.
[15] M. Garcia-Lechuga, J. Solis, and J. Siegel: Appl. Phys. A., 124, (2018) 221.
[16] S.H. Møller, S.T. Andersen, and P. Balling: Phys. Rev. Res., 2, (2020) 043010.
[17] M. Garcia-Lechuga, L. Haahr-Lillevang, J. Siegel, P. Balling, S. Guizard, and J. Solis: Phys. Rev. B., 95, (2017) 214114.
[18] J.M. Liu: Opt. Lett., 7, (1982) 196.

(Received: June 30, 2021, Accepted: December 25, 2021)